Modelling Inherent Damping for Rocking Systems: Results of Large-Scale Shake Table Testing

L. Wiebe & C. Christopoulos
University of Toronto, Canada

R. Tremblay & M. Leclerc
École Polytechnique de Montréal, Canada

SUMMARY:
This paper evaluates some common damping assumptions for modelling recent large-scale shake table tests of a controlled rocking steel frame. The most consistently accurate model for these tests assumed 2% damping at the first-mode period and at five times that period, using the tangent stiffness matrix. The results of numerical modelling were much more sensitive to the inherent damping than they were to the initial stiffness of the frame. Because inherent damping still cannot be predicted reliably, design decisions should not rely on how damping is modelled. Comparing the results of 760 numerical analyses to 76 large-scale shake table tests demonstrated that mitigating higher mode effects in a controlled rocking steel frame reduces the sensitivity of calculated forces to damping assumptions. Thus, not only can higher mode mitigation reduce peak seismic force demands, but it can also make capacity design more reliable by providing better control over those demands.

Keywords: inherent damping, controlled rocking steel frames, higher mode effects, capacity design

1. INTRODUCTION

Over the last twenty years, as the computational tools that are available to earthquake engineers have become much more accessible, engineers have come to rely more on numerical modelling for both research and design. One important aspect of a numerical model is inherent damping, which represents all energy dissipation that is not modelled explicitly. The three main sources of this damping are soil-foundation-structure interaction, non-structural elements, and slightly nonlinear response in elements that are modelled linearly (Priestley and Grant 2005). Damping in the first mode decreases with increasing period, but the scatter is high (Satake et al. 2003). Damping in the higher modes is believed to be equal to (O'Rourke 1976) or greater than (Satake et al. 2003) damping in the first mode.

The uncertainty of the numerical value of damping is compounded by the lack of consensus on how to model it. Classical viscous damping is often assumed because it allows a linear multi-degree-of-freedom (MDOF) system to be analyzed using modal analysis. Rayleigh damping is often assumed, where the damping matrix, $\mathbf{c}$, is calculated from the mass matrix, $\mathbf{m}$, and the stiffness matrix, $\mathbf{k}$, as:

$$\mathbf{c} = \alpha\mathbf{m} + \left(\beta_{\tan}\mathbf{k}_{\tan} + \beta_0\mathbf{k}_0\right) \tag{1.1}$$

where α and β are the mass- and stiffness-proportional damping coefficients, and where $\tan$ and 0 refer to the tangent and initial stiffness matrices, respectively. For linear systems, $\left(\beta_{\tan}\mathbf{k}_{\tan} + \beta_0\mathbf{k}_0\right)$ is rewritten as $\beta\,\mathbf{k}$ because $\mathbf{k}_{\tan} = \mathbf{k}_0$. In this case, the damping ratio ξ at any frequency ω is given by:

$$\xi = \frac{\alpha}{2\omega} + \frac{\beta\omega}{2} \tag{1.2}$$

By adjusting the coefficients α and β, the damping ratio at any two frequencies can be selected.

Some form of Eqn. 1.1 is commonly assumed even when modal analysis is not used because of nonlinear response. Léger and Dussault (1992) have defined three groups of Rayleigh damping models for nonlinear time-history analysis based on how the damping matrix is calculated as the stiffness matrix changes. In the first group, the damping matrix uses only the initial system properties and is constant: $\beta_{\tan} = 0$. In the second group, $\beta_0 = 0$, and both α and $\beta_{\tan}$ are constant. In the third group, $\beta_0 = 0$, and both α and $\beta_{\tan}$ are recomputed as the instantaneous modal properties change. Charney (2008) has described the effect of stiffness changes on MDOF systems using each of these models. However, there is no consensus on which approach is the most appropriate, or even if a viscous damping model should be used at all. Therefore, the purpose of this paper is to examine the influence of damping assumptions on the ability of a numerical model to capture the measured response from a large number of recent large-scale shake table tests of a controlled rocking steel frame.

2. CONTROLLED ROCKING STEEL FRAMES

In a controlled rocking steel frame, the column bases are allowed to lift off the foundation rather than developing tension. Unbonded post-tensioning is often used to adjust the lateral load that will cause the frame to rock and to provide a positive global stiffness during rocking, and supplemental energy dissipation that is activated by rocking is typically used to limit the peak response. Christopoulos et al. (2002) have shown that flag-shaped hystereses, which are characteristic of controlled rocking systems, can be designed to have a peak response that is similar to the response of systems with elastoplatic hystereses, while also avoiding structural damage and residual deformations. A number of experimental studies of controlled rocking steel frames for buildings have confirmed that they are able to reduce or eliminate structural damage and residual deformations during large-amplitude ground motions (Clough and Huckelbridge 1977, Kelly and Tsztoo 1977, Midorikawa et al. 2003, Tremblay et al. 2008, Eatherton et al. 2010, Ma et al. 2010, Sause et al. 2010, Wiebe et al. 2012).

Unlike the braces of a concentrically braced frame, which are intended to yield, all elements of a controlled rocking steel frame are intended to remain elastic while the base rocking response limits the seismic demand. Previous numerical studies (Roke et al. 2009, Eatherton and Hajjar 2010) have shown that the elastic forces for members of rocking frames are strongly influenced by higher mode effects. As an alternative to strengthening these members to resist the elastic force demands, Wiebe et al. (2012) proposed two techniques for mitigating higher mode effects in rocking frames and validated those techniques by shake table testing of an eight-storey controlled rocking steel frame at 30% scale. This paper uses those tests as an experimental reference for evaluating inherent damping assumptions.

3. SHAKE TABLE TEST PROGRAM

3.1. Design of Shake Table Test Structure

Figure 1 gives an overview of the test setup. The test frame was designed based on an eight-storey office building in Vancouver, BC. The building was 27m x 27m with 9m bays and four rocking frames in each direction. The seismic weight was calculated based on 4.2 kPa of dead load, while gravity loads were carried by adjacent members. Because the post-uplift stiffness of a rocking frame can be chosen independently of the rocking load, the frame was not designed based on a force reduction factor. Instead, it was designed to reach the same base moment at 2% roof drift as a code-compliant buckling-restrained braced frame. Half of this moment was resisted by friction energy dissipation, while post-tensioning resisted the remainder. The design was scaled to 30% using similitude relations for artificial mass simulation (Harris and Sabnis 1999). The members were sized using nonlinear time-history analyses to ensure that the structure would not be damaged by large-amplitude tests. The mass simulation system used pinned columns between floors to include P-Δ effects. The pin-ended struts that connected the mass system to the test frame included load cells to measure the inertia forces, which were integrated to find the storey shears and overturning moments.

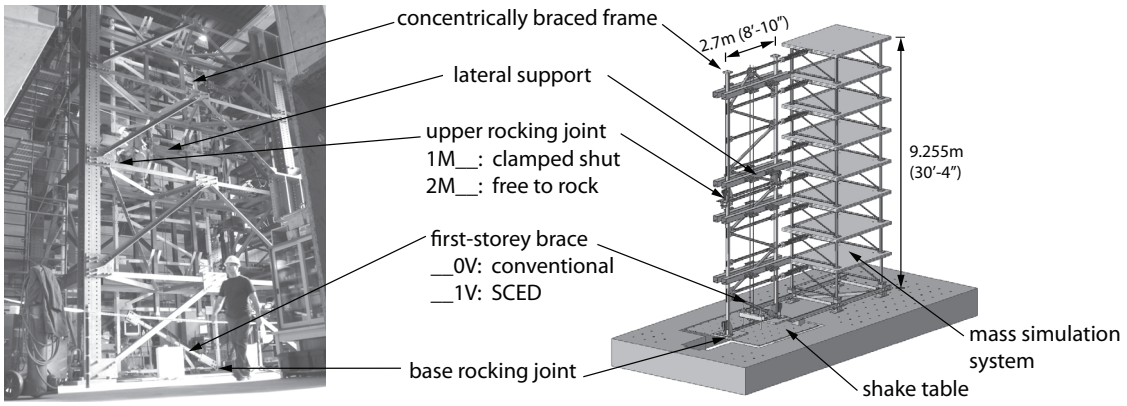

Figure 1. Controlled rocking steel frame shake table test setup

3.2. Higher Mode Mitigation

The frame was tested in four different configurations in order to evaluate two higher mode mitigation techniques. In the 1M0V configuration, rocking was permitted only at the base, and conventional braces were used throughout. In the 2M0V configuration, a second rocking joint was used to better control the moment immediately above the fourth storey (approximately midheight). The energy dissipation at this joint was designed to be half that at the base in order to target a linear distribution of moments from the base of the structure to the roof. In the 1M1V configuration, the first-storey brace was replaced with a self-centering energy dissipative (SCED) brace (Christopoulos et al. 2008) that was designed to activate at the base shear that would cause rocking according to the code-based lateral force distribution. Finally, the 2M1V configuration combined both higher mode mitigation techniques.

3.3. Sources of Damping

The shake table tests are expected to be a lower bound to the damping in a built structure. Although material damping may be similar for both, the gravity system is not modelled in the shake table test program, and the shake table likely provides less foundation damping than in practice. Although non-structural elements are not included in the test setup, friction with the lateral supports contributes to damping in the test structure. Greased PTFE pads were used for lateral supports at four locations, as shown in Fig. 1. Quasi-static testing showed a total of less than 5 kN of friction between the rocking frame and the lateral supports. This is only about 2% of the peak measured base shear of 219 kN.

3.4. Suite of Base Excitations

The test program included two historical ground motions at the service hazard level for Vancouver (50% / 50 yrs), three at the design level (10% / 50 yrs, DBE), and three at the maximum considered level (2% / 50 yrs, MCE). Two slightly modified historical records were used for the Cascadia subduction scenario (84th percentile of 2% / 50 yrs), and one spectrally-matched historical record and one synthetic record were used for eastern North America (2% / 50 yrs in Montreal). Finally, one MCE record was incrementally scaled by factors ranging from 25% to 200% (INC). Of these 19 ground motions, Table 1 summarizes the properties only for records DBE-3 and INC-200%, since this paper uses them to demonstrate the response to medium- and large-amplitude earthquakes. In addition to the seismic records, a sinusoidal acceleration pulse with a frequency of 1 Hz was used to displace the structure to a roof drift of approximately 2.5%, after which the frame responded in free vibration.

Table 1. Summary of ground motions

ID	earthquake	station	M	distance (km)	azimuth	scale
DBE-3	Loma Prieta (1989)	Bear Valley #5	6.9	76	310	1.70
INC-200%	Manjil, Iran (1990)	Abbar	7.4	43	TRANS	2.00

4. NUMERICAL MODEL

Figure 2 shows the OpenSees (2011) numerical model of the shake table test structure. Nonlinear fibre elements are used for all beam and column elements, and rigid offsets are included for the beams. Corotational truss elements are used for all braces, mass simulation system elements, and for the post-tensioning, which also has an initial strain. Gap elements with a compression stiffness of 1000 kN/mm are used together with elastic-perfectly plastic elements to represent the uplift and friction response at the rocking joints. One node at the base of the structure is constrained horizontally to transfer the base shear. When the upper joint is not free to rock (1M configurations), the gap elements at the upper joint are replaced with rigid links, while when it is free to rock (2M configurations), an element with a high shear stiffness but negligible axial stiffness is used. The self-centering material property is used for the SCED brace in 1V configurations. All masses are lumped at the nodes, with most of the mass occurring in the mass simulation system. A Krylov-Newton solution algorithm provided the most stability in computing the response. The initial frequency of the numerical model (2.08 Hz) was within 2% of the value determined from low-amplitude testing (2.05 Hz).

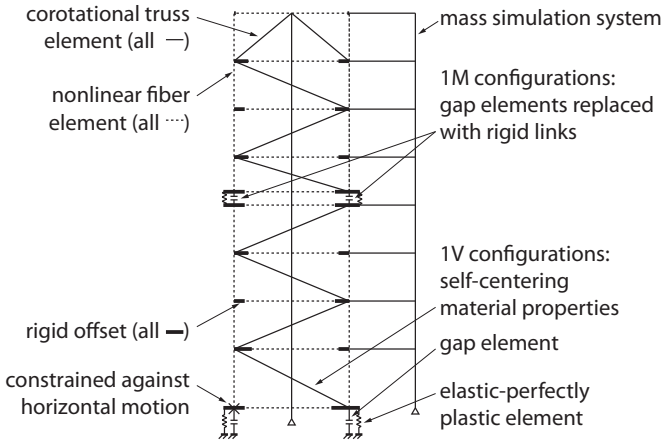

Figure 2. Schematic of numerical model

5. EVALUATION OF DAMPING MODELS FOR 1M0V CONFIGURATION

The model was less sensitive to stiffness assumptions than it was to damping assumptions. To demonstrate this, Fig. 3 shows the response of three models of the 1M0V configuration to the DBE-3 and INC-200% records. The models are intended to bracket the range of periods that an analyst might calculate: one model has a first-mode period of 0.48 s (as described above), one has a lower bound period of 0.41 s (obtained by adding rigid offsets to the column connections and increasing the gap element stiffness), and one has an upper bound period of 0.51 s (obtained by removing the rigid offsets from the beam elements and assuming that all elements have the minimum allowable cross-sectional properties). Tangent stiffness Rayleigh damping of 2% is applied at the first-mode period and at five times that period for the reasons that are given in Sec. 5.5. Figures 3 (a)-(b) and (d)-(e) show that the calculated storey shears and overturning moments are not sensitive to these stiffness changes. The roof displacement response to record DBE-3 is larger for the more flexible model than for the stiffer models (Fig. 3 (c)), but the response to record INC-200% is nearly unchanged by varying stiffness assumptions (Fig. 3 (f)) because the system behaves as a rigid rocking body at large amplitudes.

Because the numerical results are relatively insensitive to the model stiffness, only the model with a period of 0.48 s is used for the following analyses. The only change between models is in the representation of the inherent damping that comes from the sources that were given in Sec. 3.3. In order to highlight the difference between damping models, the influence of damping is intentionally overestimated by assuming a damping ratio of 10%. Only damping of the form given in Eqn. 1.1 is considered because of the limitations of the analysis platform (OpenSees 2011).

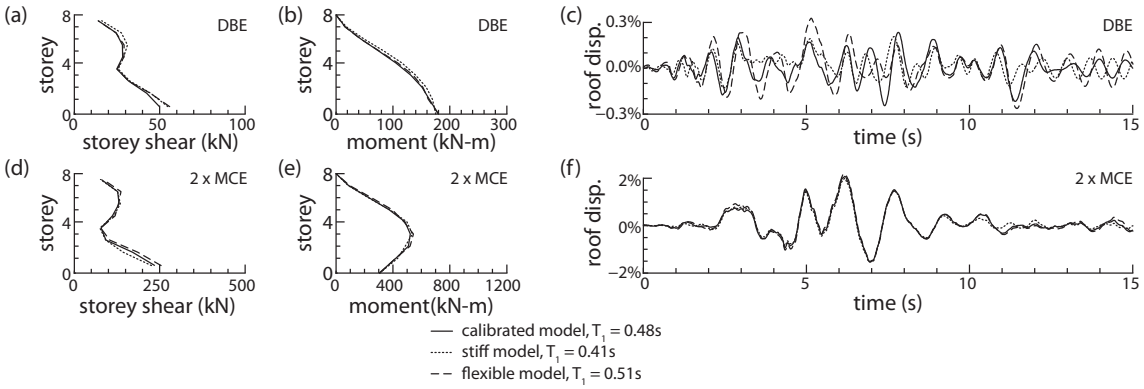

Figure 3. Numerical response with varying model stiffness: (a) storey shear envelope for DBE-3; (b) overturning moment envelope for DBE-3; (c) roof displacement response for DBE-3; (d) storey shear envelope for INC-200%; (e) overturning moment envelope for INC-200%; (f) roof displacement response for INC-200%

5.1. Rayleigh Damping in Modes 1 and 2 with Tangent Stiffness Matrix

Figure 4 compares the experimental results with the numerical results assuming equal damping in modes 1 and 2 of either 0.4% or 10%. Figure 4 (a) shows the associated damping at other frequencies based on Eqn. 1.2. For both models, the damping matrix was computed using the stiffness matrix from the end of the previous time step to avoid iterating the damping matrix within each time step. For the time step of 0.005s that was used, this model produced results that were practically identical to using the stiffness matrix from the current time step. Figure 4 (b) shows that assuming 0.4% damping produced a good match with the free vibration response, while the response damped out too quickly with 10% damping. However, Figs. 4 (c)-(d) and (f)-(g) show that assuming 0.4% damping in modes 1 and 2 greatly overestimates the peak seismic shears and overturning moments, while 10% damping estimates the peak forces reasonably well. Like the free vibration response, the roof displacement during seismic records is underestimated by the 10% damping model. The 0.4% model generally overshoots the displacement response to record DBE-3 (Fig. 4 (e)), and it also overestimates the number of cycles of free vibration after the end of the records, but there is good agreement for the displacement response to record INC-200% (Fig. 4 (h)).

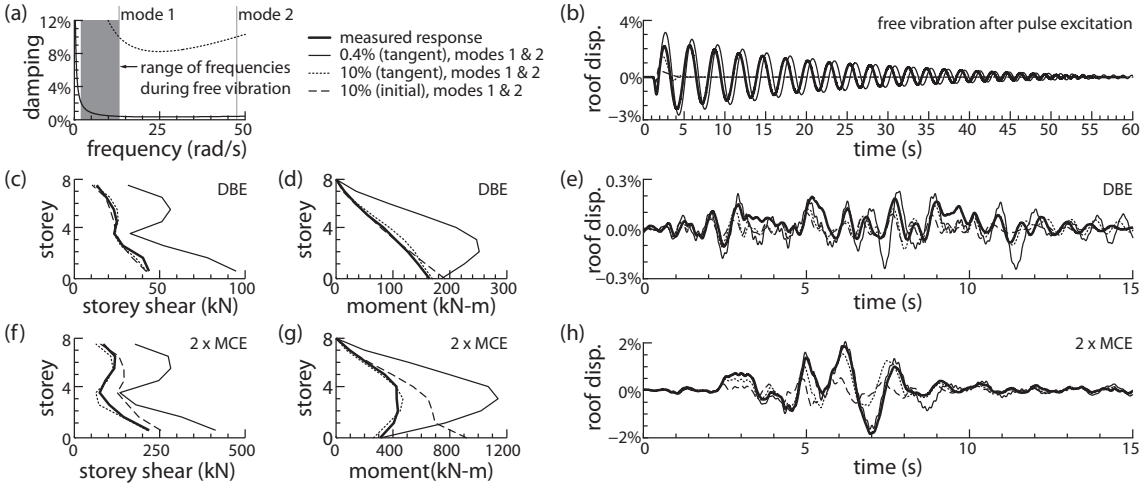

Figure 4. Experimental and numerical response with damping specified in modes 1 and 2: (a) damping vs. frequency; (b) roof displacement response in free vibration; (c) storey shear envelope for DBE-3; (d) overturning moment envelope for DBE-3; (e) roof displacement response for DBE-3; (f) storey shear envelope for INC-200%; (g) overturning moment envelope for INC-200%; (h) roof displacement response for INC-200%

5.2. Rayleigh Damping in Modes 1 and 2 with Initial Stiffness Matrix

Figure 4 also shows the response when the initial stiffness matrix is used to define Rayleigh damping of 10% in modes 1 and 2. This model both underestimates the displacements (Figs. 4 (b), (e), and (h)) and overestimates the sectional forces at large amplitudes (Figs. 4 (f) and (g)). The base moment during the INC-200% record is particularly overestimated by this model because of large damping forces in the gap elements. This confirms Charney's recommendation (2008) that initial stiffness damping should not be assigned to nonlinear elements with high initial stiffness. An analyst is unlikely to accidentally assign damping to a gap element using OpenSees (2011) because no damping is the default option for zero-length and linear truss elements. For a rocking system where most elements behave elastically, there is effectively no difference between initial-stiffness and tangent-stiffness damping if the gap elements are assigned zero damping.

5.3. Rayleigh Damping in Modes 1 and 8 with Tangent Stiffness Matrix

To avoid overdamping the higher modes, Carr (2007) has recommended that if Rayleigh damping is used, it should be based on the first mode and a mode near the number of storeys. Comparing Figs. 4 and 6, the displacements with 10% damping in modes 1 and 8 are similar to those with 10% damping in modes 1 and 2 because the two methods give similar damping at low frequencies (Figs. 4 (a) and 6 (a)). The sectional forces, which are more influenced by the higher modes, are larger when the damping in the higher modes is reduced, as shown in Figs. 5 (c)-(d) and (f)-(g). For this structure, 10% damping in modes 1 and 8 underestimates the displacements but overestimates the sectional forces.

5.4. Damping Proportional to Tangent Stiffness Only

Priestley et al. (2007) have proposed using only tangent stiffness-proportional damping (i.e. $\alpha = 0$ in Eqn. 1.1). Figure 5 (a) shows that assuming 10% damping in mode 1 implies much less damping at lower frequencies. While the peak displacement due to the pulse excitation is overestimated, the rate of decay of free vibration is modelled well (Fig. 5 (b)). The peak displacement is also overestimated for the DBE-3 record (Fig. 5 (e)), but the displacements are modelled well overall for both that record and the larger INC-200% record (Fig. 5 (h)). However, because this model produces high damping in the higher modes, it underestimates the peak storey shears. Reducing the assumed damping would improve the agreement for the sectional forces but would further overestimate the displacements.

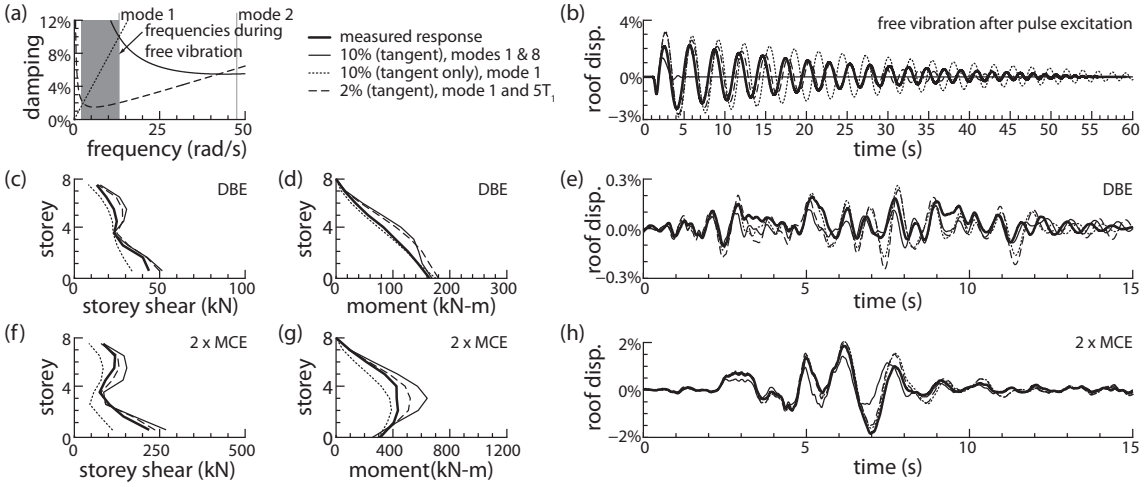

Figure 5. Experimental and numerical response with other Rayleigh damping models: (a) damping vs. frequency; (b) roof displacement response in free vibration; (c) storey shear envelope for DBE-3; (d) overturning moment envelope for DBE-3; (e) roof displacement response for DBE-3; (f) storey shear envelope for INC-200%; (g) overturning moment envelope for INC-200%; (h) roof displacement response for INC-200%

5.5. Alternative Rayleigh Damping Models with Tangent Stiffness Matrix

The above results suggest that low damping is required at low frequencies to match the displacements, while more damping is required at higher frequencies to match the sectional forces. Therefore, Rayleigh damping models with more damping in mode 2 than mode 1 were considered. The Rayleigh damping model causes negative damping at some frequencies if the following relation is not followed:

$$\frac{\omega_1}{\omega_2} \leq \frac{\xi_2}{\xi_1} \leq \frac{\omega_2}{\omega_1} \tag{5.1}$$

where $\omega_2 > \omega_1$ are the two frequencies for which the damping ratio is specified. These analyses are not presented because they did not substantially improve the numerical results.

The apparent first-mode frequency of a rocking system increases as the response amplitude decreases. A logarithmic decrement approach between successive peaks in free vibration gave 2% damping for all but the smallest cycles. To model this, a tangent-stiffness Rayleigh damping model was developed with 2% damping at the highest and lowest apparent frequencies in free vibration (1.70 and 0.32 Hz). A simplified recommendation using the initial frequency of the numerical model and one fifth of that frequency (2.08 and 0.41 Hz) gave very similar results, so only the latter model is presented. Figures 5 (b) and (h) show that this model captures the displacements in free vibration and during the INC-200% record, but Fig. 5 (e) shows that the model overestimates the peak displacement during record DBE-3. The model also slightly overestimates the sectional forces (Figs. 5 (c)-(d) and (f)-(g)). Whereas other models captured either the forces or the displacements, but not both, this model provides fair matches for both. It is not clear whether this damping model would work equally well for a full building.

5.6. Explicit Modelling of Damping

Friction between the frame and the lateral supports was explicitly modelled by elastic-perfectly plastic elements between the model and fixed reference nodes at the levels nearest the four supports. The slip loads for these elements were based on quasi-static testing. Multiple support excitation was used to prevent the reference nodes from moving with the base. The inherent damping was reduced to 0.1% for the models in Fig. 6, but other models with more inherent damping were also considered. The first model in Fig. 6 has a slip load of 1 kN at each lateral support, while the second increases the slip loads to as much as 10 kN because the first model overestimated the peak forces (Figs. 6 (c)-(d) and (f)-(g)). Both models damp out too quickly in free vibration (Fig. 6 (b)), only the first model captures the displacements during records DBE-3 (Fig. 6 (e)) and INC-200% (Fig. 6 (h)), and the second model has a residual displacement after record DBE-3. While the second model matches the force envelopes well for record DBE-3 (Figs. 6 (c)-(d)), it overestimates them during the larger INC-200% record (Figs. 6 (f)-(g)). Although friction with the lateral supports is believed to be a significant damping source for these tests, this friction depends on the normal force between the frame and the supports, it may be rate-dependent, and it may also vary with the location and direction of motion of the frame. Current modelling capabilities do not capture these influences well enough for explicit modelling of friction with the lateral supports to improve the results relative to more conventional damping models.

6. DAMPING SENSITIVITY FOR DIFFERENT CONFIGURATIONS

This section examines the sensitivity of numerical models for all four configurations that were tested. Inherent damping is modelled with a Rayleigh damping model based on the tangent stiffness matrix with equal damping in the first two initial modes. For all 19 ground motions in all four configurations, analyses were conducted using 10 values of damping from 0.1% to 10%. Figure 7 summarizes the results of these 760 numerical analyses. On the vertical axis of each plot is the ratio of the numerical estimate to the measured result for one response parameter, and on the horizontal axis of each plot is the assumed damping ratio. Each column of plots corresponds to one configuration.

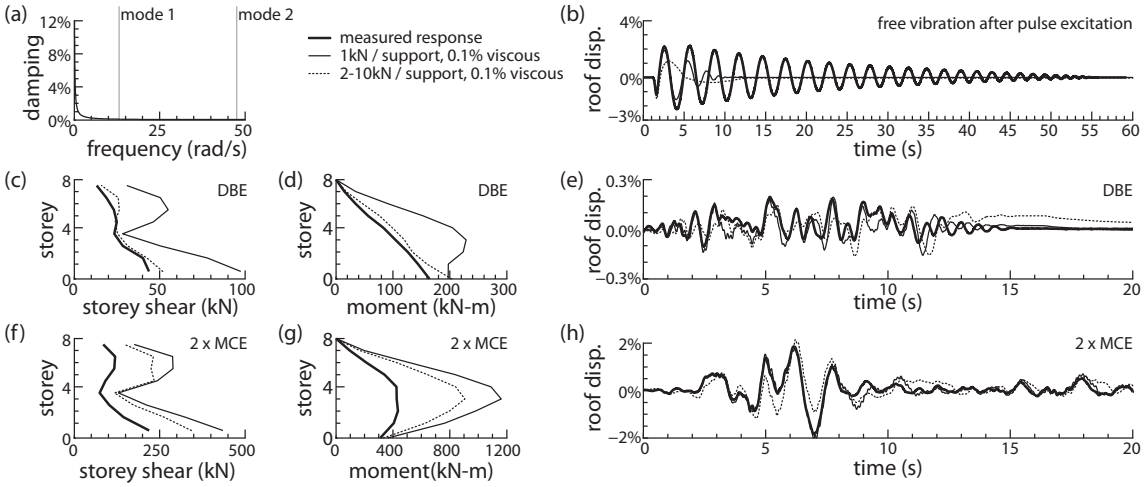

Figure 6. Experimental and numerical response with explicit modelling of lateral support friction: (a) damping vs. frequency; (b) roof displacement response in free vibration; (c) storey shear envelope for DBE-3; (d) overturning moment envelope for DBE-3; (e) roof displacement response for DBE-3; (f) storey shear envelope for INC-200%; (g) overturning moment envelope for INC-200%; (h) roof displacement response for INC-200%

The first row of plots in Fig. 7 gives the ratio of calculated to experimentally observed peak base shear. The calculated shear in the base-rocking only (1M0V) configuration is sensitive to damping (lines are steep), the model is usually conservative (ratio greater than 1), and the accuracy varies between ground motions (lines are spread apart). With a SCED brace at the first storey (1M1V), there is less sensitivity to damping (lines are less steep) and less variability in accuracy between records (lines are clustered more tightly). Relative to base-rocking only (1M) configurations, configurations with an upper rocking joint (2M) are less sensitive to damping, but more variable in accuracy. In addition to these changes in sensitivity and variability, higher mode mitigation reduces the base shears (Wiebe et al. 2012). For example, the base shears in the 2M0V and 1M1V configurations are lower by averages of 12% and 37%, respectively, relative to the 1M0V configuration.

The second row of plots in Fig. 7 gives the ratio of calculated to observed peak overturning moment at the location of the upper rocking joint in the 2M configurations. The upper rocking joint reduced the peak overturning moment at this location (Wiebe et al. 2012). Figure 7 shows that the higher mode mitigation also reduced the sensitivity of this parameter to damping, as shown by the reduced slope of the lines. The variability in the 2M configurations is also less than in the 1M configurations.

The third row of plots in Fig. 7 gives the ratio of calculated to observed peak column compression at the fourth storey. This compression comes from the overturning moment (second row of plots) and the vertical load. The known vertical load causes the peak compression to be more consistently accurate than the peak overturning moment. Like the other parameters, the compression in the 1M0V configuration is more sensitive to damping than for the configurations with higher mode mitigation.

The bottom row of plots in Fig. 7 gives the ratio of calculated to observed peak roof displacement. Although the peak roof displacement was not greatly influenced by higher mode mitigation (Wiebe et al. 2012), the sensitivity to assumed damping and the variability of accuracy with ground motion are both slightly less for the configurations with higher mode mitigation than for the 1M0V configuration.

Comparing the four rows of plots, the sets of lines do not generally cross unity at the same damping ratio, particularly for the 1M0V configuration. This suggests that the assumed damping model does not accurately capture the physical damping phenomena, since no single damping ratio results in correct estimates of all four parameters. The improvement in this for the other configurations suggests that they are less sensitive not only to the numerical value of damping, but also to how it is modelled.

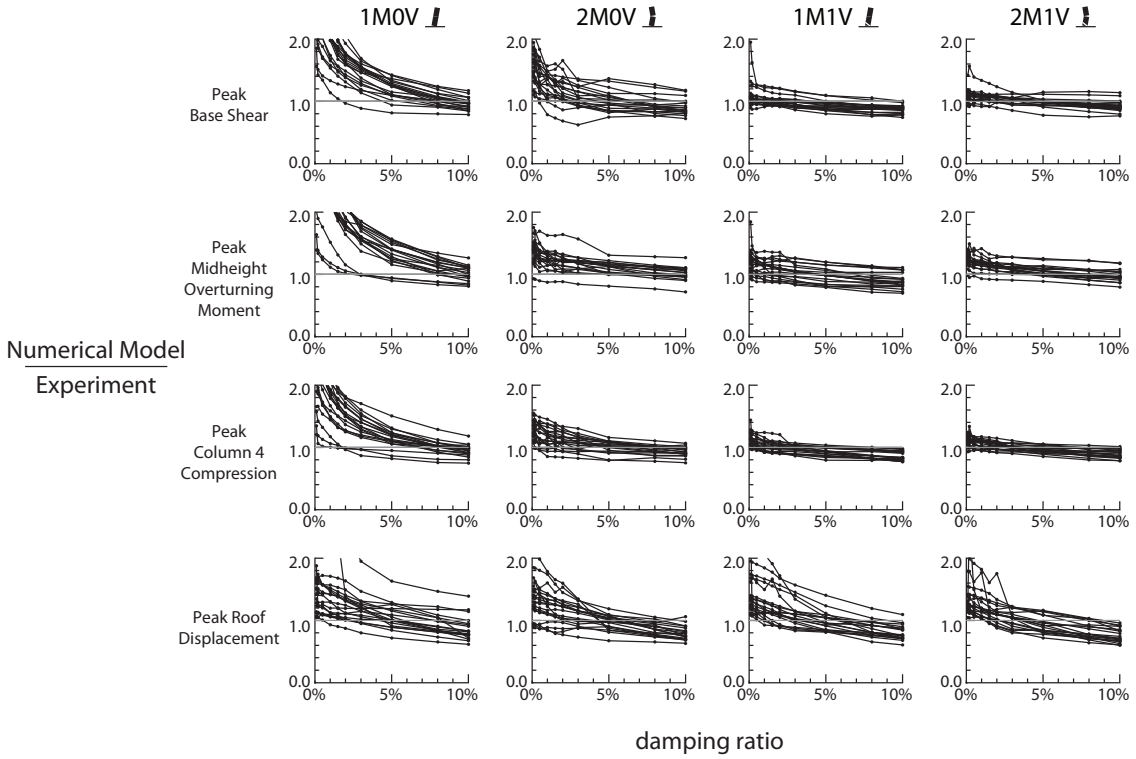

Figure 7. Sensitivity of response to damping ratio, tangent-stiffness Rayleigh damping, equal in modes 1 and 2

7. CONCLUSIONS

Recent shake table testing of a controlled rocking steel frame with significant higher mode effects was used as a benchmark to evaluate a variety of common damping assumptions. The assumed inherent damping influenced the numerical modelling results more than any reasonable assumptions that could be made about the model stiffness. Most Rayleigh damping models could not capture both the roof displacement response (dominated by low frequencies) and sectional forces (dominated by higher frequencies) over the full range of amplitudes that were tested. The best results assumed 2% damping at the initial first-mode period and at five times that period, using tangent stiffness Rayleigh damping. However, this result may not be generally applicable, and these shake table test specimens are expected to have less inherent damping than a built structure. Initial stiffness damping should not be applied to gap elements. Explicit modelling of damping due to friction with the lateral supports did not improve the agreement between the experimental and numerical models.

Considering the wide range of inherent damping assumptions that an analyst could make, decisions that are made based on the results of numerical modelling must be robust with respect to those assumptions. Comparing the results of 760 numerical analyses to 76 large-scale shake table tests demonstrated that mitigating higher mode effects in a controlled rocking steel frame reduces the sensitivity of calculated forces to damping assumptions, as well as the variability in the accuracy of calculated forces across different ground motions. Higher mode effects can be mitigated by providing multiple force-limiting mechanisms, such as multiple rocking joints or nonlinear braces. In general, where higher mode effects can make capacity design unreliable because of the uncertainty in the lateral force distribution at the instant of peak response, it is expected that mitigating higher mode effects can make capacity design more reliable by providing better control over peak forces.

ACKNOWLEDGMENT

Funding for this project was provided by the Natural Sciences and Engineering Research Council of Canada, the Canadian Seismic Research Network, the Ontario Ministry of Research and Innovation, and the Fonds de Recherche du Québec sur la Nature et les Technologies. Dungil Rubber Belt Co. (Busan, Korea) fabricated the SCED brace. Lainco Inc. (Terrebonne, Quebec) and the Canadian Institute of Steel Construction contributed to the shake table test setup. The contributions of the staff and students at the Laboratoire de Structures Hydro-Québec de l'École Polytechnique of Montréal are also gratefully acknowledged.

REFERENCES

Carr, A.J. (2007). Ruaumoko manual, Volume 1: theory. University of Canterbury, Christchurch, New Zealand.

Charney, F.A. (2008). Unintended consequences of modeling damping in structures. *J. Struct. Eng.* **134: 4**, 581-592.

Christopoulos, C., Filiatrault, A., and Folz, B. (2002). Seismic response of self-centring hysteretic SDOF systems. *Earthquake Eng. Struct. Dyn.* **31: 5**, 1131-1150.

Christopoulos, C., Tremblay, R., Kim, H.-J., and Lacerte, M. (2008). Self-centering energy dissipative bracing system for the seismic resistance of structures: development and validation. *J. Struct. Eng.* **134: 1**, 96-107.

Clough, R.W., and Huckelbridge, A.A. (1977). Preliminary experimental study of seismic uplift of a steel frame. UCB/EERC Report 77/22, Earthquake Eng. Research Centre, Berkeley, CA.

Eatherton, M., and Hajjar, J. (2010). Large-scale cyclic and hybrid simulation testing and development of a controlled-rocking steel building system with replaceable fuses. NSEL Report NSEL-025, Dept. of Civil and Env. Eng., Univ. of Illinois at Urbana-Champaign.

Eatherton, M., Hajjar, J., Ma, X., Krawinkler, H., and Deierlein, G. (2010). Seismic design and behavior of steel frames with controlled rocking – Part I: concepts and quasi-static subassembly testing. *Proc., ASCE/SEI Structures Congress 2010*, Orlando, FL.

Harris, H.G., and Sabnis, G.M. (1999). Structural modeling and experimental techniques, 2nd ed., CRC Press LLC, Boca Raton, FL.

Kelly, J.M., and Tsztoo, D.F. (1977). Earthquake simulation testing of a stepping frame with energy-absorbing devices. UCB/EERC Report 77/17, Earthquake Eng. Research Centre, Berkeley, CA.

Léger, P., and Dussault, S. (1992). Seismic-energy dissipation in MDOF structures. *J. Struct. Eng.* **118: 5**, 1251-1269.

Ma, X., Deierlein, G., Eatherton, M., Krawinkler, H., Hajjar, J., Takeuchi, T., Kasai, K., Midorikawa, M., and Hikino, T. (2010). Seismic design and behavior of steel frames with controlled rocking - Part II: Large scale shake table testing and system collapse analysis. *Proc., ASCE/SEI Structures Congress 2010*, Orlando, FL.

Midorikawa, M., Azuhata, T., Ishihara, T., Matsuba, Y., and Wada, A. (2003). Shaking table tests on earthquake response reduction effects of rocking structural systems. *Proc., Smart Structures and Materials 2003: Damping and Isolation (SPIE Vol. 5052)*. San Diego, CA.

National Research Council of Canada (NRCC). (2005). National building code of Canada, 12th ed., NRCC, Ottawa, ON.

O'Rourke, M. (1976). Discussion of Response to stochastic wind of N-degree tall buildings. *ASCE J. Struct Div.* **102: ST12**, 2401-2403.

OpenSees. (2011). Open system for earthquake engineering simulation (OpenSees), v 2.3.2. Computer software. Pacific Earthquake Engineering Research Center, Berkeley, CA.

Priestley, M.J.N., Calvi, G.M., and Kowalsky, M.J. (2007). Displacement-based seismic design of structures. IUSS Press, Pavia, Italy.

Priestley, M.J.N., and Grant, D.N. (2005). Viscous damping in seismic design and analysis. *J. Earthquake Eng.* **9: SP2**, 229-255.

Roke, D., Sause, R., Ricles, J.M., and Gonner, N. (2009). Damage-free seismic-resistant self-centering steel concentrically-braced frames. *Proc., STESSA 2009*, Philadelphia, PA.

Sause, R., Ricles, J.M., Roke, D.A., Chancellor, N.B., and Gonner, N.P. (2010). Seismic performance of a self-centering rocking concentrically braced frame. *Proc., 9th US National and 10th Can. Conf. on Earthquake Eng.*, Toronto, ON.

Satake, N., Suda, K., Arakawa, T., Sasaki, A., and Tamura, Y. (2003). Damping evaluation using full-scale data of buildings in Japan. *J. Struct. Eng.* **129: 4**, 470-477.

Tremblay, R., Poirier, L.-P., Bouaanani, N., Leclerc, M., Rene, V., Fronteddu, L., and Rivest, S. (2008). Innovative viscously damped rocking braced steel frames. *Proc., 14th World Conf. on Earthquake Eng.*, Beijing, China.

Wiebe, L., Christopoulos, C., Tremblay, R., and Leclerc, M. (2012). Shake table testing of a rocking steel frame designed to mitigate higher mode effects. *Proc., STESSA 2012*, Santiago, Chile.